An Insertion Mutation That Distorts Antibody Binding Site Architecture Enhances Function of a Human Antibody

Jens C. Krause,[a] Damian C. Ekiert,[b] Terrence M. Tumpey,[c] Patricia B. Smith,[a] Ian A. Wilson,[b] and James E. Crowe, Jr.[a,d]

Department of Pediatrics, Vanderbilt University Medical Center, Nashville, Tennessee, USA[a]; Department of Molecular Biology and the Skaggs Institute for Chemical Biology, The Scripps Research Institute, La Jolla, California, USA[b]; Influenza Division, Centers for Disease Control and Prevention, Atlanta, Georgia, USA[c]; and Department of Microbiology and Immunology, Vanderbilt University Medical Center, Nashville, Tennessee, USA[d]

J.C.K. and D.C.E. contributed equally to this article.

ABSTRACT **The structural and functional significance of somatic insertions and deletions in antibody chains is unclear. Here, we demonstrate that a naturally occurring three-amino-acid insertion within the influenza virus-specific human monoclonal antibody 2D1 heavy-chain variable region reconfigures the antibody-combining site and contributes to its high potency against the 1918 and 2009 pandemic H1N1 influenza viruses. The insertion arose through a series of events, including a somatic point mutation in a predicted hot-spot motif, introduction of a new hot-spot motif, a molecular duplication due to polymerase slippage, a deletion due to misalignment, and additional somatic point mutations. Atomic resolution structures of the wild-type antibody and a variant in which the insertion was removed revealed that the three-amino-acid insertion near the base of heavy-chain complementarity-determining region (CDR) H2 resulted in a bulge in that loop. This enlarged CDR H2 loop impinges on adjacent regions, causing distortion of the CDR H1 architecture and its displacement away from the antigen-combining site. Removal of the insertion restores the canonical structure of CDR H1 and CDR H2, but binding, neutralization activity, and *in vivo* activity were reduced markedly because of steric conflict of CDR H1 with the hemagglutinin antigen.**

IMPORTANCE **Antibody diversification through VDJ gene recombination, junctional variation, and somatic hypermutation has clear importance for the generation of mature, high-affinity antibodies. Between 1.3 and 6.5% of antibody variable gene sequences have been reported to contain insertions or deletions, but their structural and functional significance remains less well defined. The pandemic influenza virus hemagglutinin antibody 2D1 data suggest that somatic insertions and deletions in antibody genes contribute important structural and functional features. We predict that such features can be critical for affinity and functional maturation of the human antibody repertoire.**

Received 31 December 2010 **Accepted** 6 January 2011 **Published** 8 February 2011

Citation Krause, J. C., D. C. Ekiert, T. M. Tumpey, P. B. Smith, I. A. Wilson, et al. 2011. An insertion mutation that distorts antibody binding site architecture enhances function of a human antibody. mBio 2(1):e00345-10. doi:10.1128/mBio.00345-10.

Editor Matthew D. Scharff, Albert Einstein College of Medicine

Address correspondence to James E. Crowe, Jr., james.crowe@vanderbilt.edu.

The breadth of antibody repertoires is shaped by combinatorial and junctional diversity during B cell ontogeny and the introduction of somatic point mutations during germinal center reactions. It has also been noted that some heavy- and light-chain genes contain somatically introduced insertions or deletions (1–5), but the functional and structural significance of such alterations in human antibodies remains unclear due to the low number of human antibodies studied to date and a paucity of crystallographic data from antibodies with such insertions or deletions.

2D1 is an IgG1/λ human monoclonal antibody (MAb) derived from a circulating B cell in the peripheral blood of a 1918 influenza pandemic survivor (6). MAb 2D1 was originally isolated as a 1918-specific antibody, which was made possible by reconstruction of the virus from RNA sequences recovered from the preserved tissues of victims (7). In April 2009, a novel influenza A H1N1 virus (2009 H1N1) caused an outbreak starting in Mexico that spread globally and developed into the first human influenza pandemic in 40 years (8). Early sequence and serological analyses suggested that the 1918 and 2009 H1N1 hemagglutinins (HAs) were antigenically similar, as parts of the four main antigenic sites (Ca, Cb, Sa, and Sb) were well conserved (9–12). Indeed, MAb 2D1 binds and neutralizes both the 1918 and 2009 H1N1 pandemic influenza viruses because the 2D1 epitope in the Sa site of the 1918 virus HA protein was conserved in swine influenza viruses for almost a century prior to its reintroduction by reassortment into a virus that caused the pandemic 2009 human outbreak (12, 13).

Previous sequence analysis revealed that MAb 2D1 was predicted to derive from the human V_H2-70 gene segment (6). In addition to conventional point mutations, the antibody also has a 9-bp insertion in framework 3 (FR3) of the heavy chain adjacent to CDR H2 (Fig. 1). The atomic resolution structure of MAb 2D1 in complex with 1918 influenza virus HA determined by X-ray crystallography revealed an unusual conformation and relative disposition of the CDR H1 and CDR H2 loops in this potent neutralizing MAb (12).

Here we describe work in which the 9-bp insertion that is

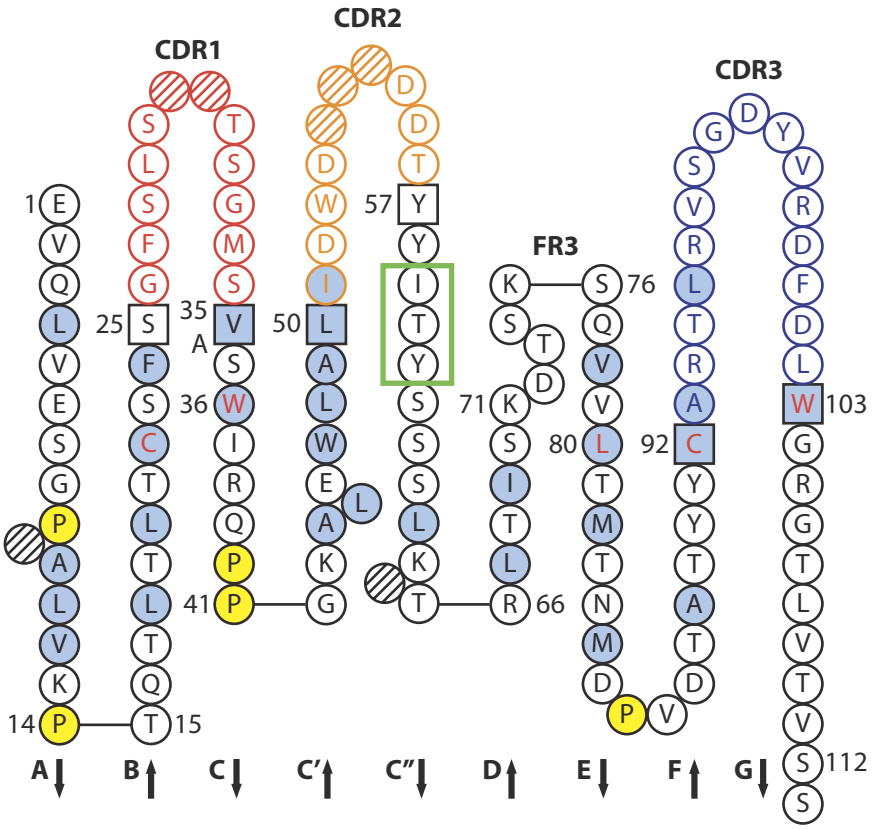

FIG 1 Amino acids of the *wt* 2D1 antibody heavy-chain variable sequences in a standard Collier de Perles two-dimensional graphic representation (28). CDR H1 is in red, CDR H2 is in orange, and CDR H3 is in slate blue. Hydrophobic amino acids and tryptophan (W), found at a given position in more than 50% of the Ig sequences analyzed, are shaded in blue. All prolines are shaded in yellow. The CDR boundaries are indicated by amino acids shown in squares. Hatched circles or squares correspond to missing positions according to the IMGT unique numbering. Arrows indicate the direction of the beta sheets and their strand designations in the three-dimensional structure. The insertion in the flanking region of *wt* 2D1 CDR H2 is indicated by a green box; the *wt* 2D1 antibody contains an ITY insertion of three amino acids in the beta strand at the base of CDR H2. This insertion was removed to generate the *del* 2D1 antibody, reflecting a reversion at that location to the predicted germ line sequence. Of note, while this illustration conforms to IMGT nomenclature and CDR definitions, the numbering is based on the Kabat numbering system to correspond to the standard positions in the crystal structures.

present in the wild-type MAb (*wt* 2D1) was removed to generate MAb *del* 2D1, thus reverting the antibody structure to a more conventional configuration characteristic of antibodies encoded by the predicted 2D1 germ line gene sequence V_H2-70. We found that removal of the insertion restored the canonical conformations of heavy-chain CDRs H1 and H2. Furthermore, comparison of the antibodies showed that acquisition of the somatic insertion during development of the mature antibody led to enhanced affinity of binding, hemagglutination inhibition (HAI) activity, and *in vivo* therapeutic activity.

RESULTS

Genetic mechanism of insertion. Retrospectively, the genetic mechanism resulting in the MAb 2D1 insertion cannot be determined with certainty; however, the most likely scenario involved a four-step process, as illustrated in Fig. 2. First, an initial somatic point mutation resulted in a change from a TA**A**A sequence to a TA**C**A sequence in an antibody gene in the V_H2-70 gene segment (Fig. 2A). This ACA sequence and another ACA sequence just 12 bp downstream (both shown in bold in Fig. 2B) likely formed the basis of a gene duplication: the second ACA triplet likely annealed with the complementary TGT triplet that would be expected to anneal with the first ACA triplet, leading to a 12-bp insertion. Subsequently, a similar misalignment during replication of the antisense strand likely resulted in a 3-bp deletion, leading to a net insertion of 9 bp (Fig. 2C). Finally, an additional two somatic point mutations occurred, resulting in the final sequence that was found in the mature *wt* 2D1 antibody gene (Fig. 2A). The genetic insertion codes for the addition of three amino acids (ITY) near the base of CDR H2 (Fig. 1).

Role of hot-spot motifs. It is of interest that the first mutation, the TA**A**A-to-TA**C**A sequence change, occurred at a previously defined somatic hypermutation hot-spot motif (the consensus sequence WA, where W is adenine or thymine and A is adenine [14]). Interestingly, the resulting mutation introduced a new hot-spot motif that occurred at the site leading to the duplication event. The TA**C**A sequence is characteristic of the WRCH consensus motif that is a strong predictor of mutability in immunoglobulin hypermutation (where W is adenine or thymine, R is the purine adenine or guanine, C is cytosine, and H is thymine, cytosine, or adenine [15]).

Effect of insertion on binding affinity. We tested whether the acquisition of the insertion affected binding affinity by comparing the binding of the original antibody with that of a mutated form of the antibody lacking the insertion. *wt* 2D1 Fab bound soluble 1918 HA with a K_D of 8.4×10^{-9} M. In contrast, the steady-state affinity of *del* 2D1 Fab was only 3.0×10^{-7} M, a marked reduction of ~35-fold. Interestingly, the effect of the insertion on affinity was mediated almost entirely by the effect on the dissociation rate. While the association rates were nearly identical (7.0×10^4/M s for *del* 2D1 versus 8.1×10^4/M s for *wt* 2D1), *del* 2D1 Fab dissociated ~30 times more readily from HA (2.1×10^{-2}/s for *del* 2D1 versus 6.8×10^{-4}/s for *wt* 2D1). It should be noted that this difference in binding was mediated only by the insertion, as we did not alter any of the predicted somatic point mutations or junctional insertions found in the *wt* 2D1 MAb.

Effect of insertion on functional activity. We next tested whether removal of the insertion affected the functional activity of the antibody. *wt* and *del* 2D1 MAbs were tested for inhibitory activity in an HAI assay against the 1918 pandemic virus [A/South Carolina/1/1918 (H1N1)], a strain of the 2009 pandemic virus [A/Mexico/4108/09 (H1N1)], and a seasonal influenza virus strain [A/Brisbane/59/07 (H1N1)] (Table 1). The 1918 and 2009 pandemic viruses share essential elements of the Sa antigenic site

FIG 2 Predicted genetic mechanism of the naturally occurring 2D1 somatic insertion/deletion. (A) Nucleotide sequences surrounding the insertion/deletion site of MAb 2D1 and its predicted germ line V_H gene segment sequence, V_H2-70. The adjacent nucleotide sequence to which the insertion/deletion is related is in bold. Shaded boxes highlight the repeat nucleotide sequence present prior to insertion/deletion. The nucleotides in the inserted sequence that likely were mutated before (in italics) or after (underlined) the insertion/deletion are indicated. (B) For the insertion to occur, the misaligned repeat sequence (in bold) created a loop and a misaligned "foot" that was extended subsequently. The nucleotides that form the basis of the deletion in panel C are in red in panel B, part 5. (C) Similarly, a misalignment in the antisense strand can lead to a deletion (according to de Wildt et al. [1]).

recognized by *wt* 2D1 antibody, but the 2007 seasonal virus possesses point mutations in that site that likely would disrupt recognition by MAb 2D1, especially the introduction of two glycosylation sites. The *wt* 2D1 and *del* 2D1 antibodies both showed significant functional activity against the 1918 and 2009 pandemic viruses but did not mediate HAI activity with the seasonal H1N1 influenza virus, as expected. The *del* 2D1 antibody mediated a 4-fold lower level of HAI activity than *wt* 2D1 against the 1918 and 2009 pandemic viruses. Mouse or ferret immune sera used as control reagents revealed the expected patterns of activity, based on previous experiments (16–19).

Effect of insertion on *in vivo* antiviral effect. We tested whether the differences in binding affinity and functional activity that we noted in these *in vitro* assays also would be seen when comparing the two antibodies *in vivo* during a lethal infection with influenza virus. In the animal model, *del* 2D1 antibody was less effective than *wt* 2D1 in reducing virus replication in the lung (Table 2). The *wt* 2D1 antibody, given at a dose of 200 μg per mouse (~10 mg/kg) at 24 h after inoculation, reduced the lung influenza virus titer over 25,000-fold compared to the human IgG control antibody preparation. In contrast, the *del* 2D1 antibody, given at the same dose, was approximately 100-fold less active *in vivo*, mediating only a 251-fold reduction in titer. *del* 2D1 was less effective than *wt* 2D1 at every dose tested.

Effect of insertion on *in vivo* therapeutic efficacy. The level of virus replication *in vivo* often correlates with disease severity due to influenza virus infection. Therefore, we tested whether the loss of antiviral potency *in vivo* for *del* 2D1 also was associated with a reduction of the therapeutic effect against weight loss and lethal infection. The results showed that *del* 2D1 was less protective against weight loss and death (Table 2; Fig. 3). At the highest dose level of the MAbs tested (200 μg), *wt* 2D1 or *del* 2D1 protected all six animals from a challenge with the virulent 1918 influenza A virus, while none of the animals in the control group treated with human IgG survived. In contrast, at the intermediate dose treatment level (20 μg), we noted a marked difference in the

TABLE 1 HAI assay results of recombinant *wt* or *del* 2D1 MAb against representative influenza A H1N1 viruses compared with those of polyclonal immune serum controls

	Sp act of MAb (μg/ml)[a]		Mean reciprocal titer of immune serum to indicated influenza A virus (species)		
H1N1 virus tested	*wt* 2D1	*del* 2D1	Mexico/4108/2009 (mouse)	South Carolina/1/1918 (ferret)	Brisbane/59/2007 (ferret)
A/South Carolina/1/1918	0.04	0.16	12	1,280	<10
A/Mexico/4108/09	0.16	0.62	1,280	400	<10
A/Brisbane/59/07	—[b]	—	—	—	640

[a] Specific HAI activity of MAbs was calculated as the lowest concentration of MAb that displayed HAI activity. Shown are the mean results of four replicate experiments.
[b] —, activity was not detected at any concentration tested, up to 5 μg/ml.

TABLE 2 Therapeutic efficacy of *wt* and *del* 2D1 MAbs against virus replication and death in mice infected with 1918 influenza A virus

MAb and dose (μg/mouse)	No. of survivors among 6 animals[a]	Mean lung virus titer ($\log_{10}$ PFU/ml) ± SD[b]	Lung virus titer reduction vs IgG control ($\log_{10}$ PFU/ml)
wt 2D1			
200	6	2.7 ± 0.6	4.4
20	6	4.6 ± 0.7	2.4
2	1	5.7 ± 0.8	1.3
del 2D1			
200	6	4.7 ± 1.0	2.4
20	2	6.1 ± 0.5	0.9
2	0	6.8 ± 0.3	0.2
Human IgG control			
200	0	7.1 ± 0.7	
20	0	7.0 ± 0.2	
2	0	7.0 ± 0.5	

[a] At the mid-dose level and the low-dose level, the differences in survival distribution between the *wt* 2D1 and *del* 2D1 groups were significant by log-rank test ($P = 0.0178$ for the mid-dose level, $P = 0.0129$ for the low-dose level).

[b] At the $\alpha = 0.0167$ level controlling the overall type I error at 5%, the lung homogenates of the *wt* 2D1 group had a lower virus titer than those of the *del* 2D1 group at the 200-μg/ml level ($P = 0.01429$) and at the 20-μg/ml level ($P = 0.01429$) by the Wilcoxon signed-rank test.

therapeutic efficacy of the antibodies when four out of six animals in the *del* 2D1 group succumbed to infection, while all of the animals in the *wt* 2D1-treated group survived.

Structural basis for enhanced affinity and function. We next sought to understand the structural basis for acquisition of the enhanced potency of *wt* 2D1 caused by the somatic insertion. We previously determined the atomic resolution structure of *wt* 2D1 Fab in complex with 1918 virus HA protein (12). Here, we obtained crystals and determined the structures of *wt* 2D1 Fab at 1.55 Å resolution and *del* 2D1 Fab at 1.65 Å resolution (Fig. 4 and 5; see Table S1 in the supplemental material). We compared the structure of *wt* 2D1 in either its bound or unbound conformation with that of a number of Fabs with similar CDR H1 amino acid sequences. While the overall structure of *wt* 2D1 resembles that of other Fabs from the Protein Data Bank (PDB), both 1918 HA-bound and free *wt* 2D1 Fabs differ markedly from sequence-related Fabs in the vicinity of CDR H1. When bound to 1918 HA, CDR H1 adopts an extended, open loop conformation (12) and appears to be quite flexible or adopt multiple conformations. Similarly, in the structure of unbound *wt* 2D1, CDR H1 adopts an extended loop conformation in one of the two copies in the asymmetric unit. In the second copy, CDR H1 is disordered, indicating conformational plasticity in this loop. In contrast, CDR H1 assumes a rigid, uniform conformation in all of the sequence-related Fab structures examined, with the middle of the loop packing back against the core of V_H, resulting in a compact, coiled configuration (Fig. 4B).

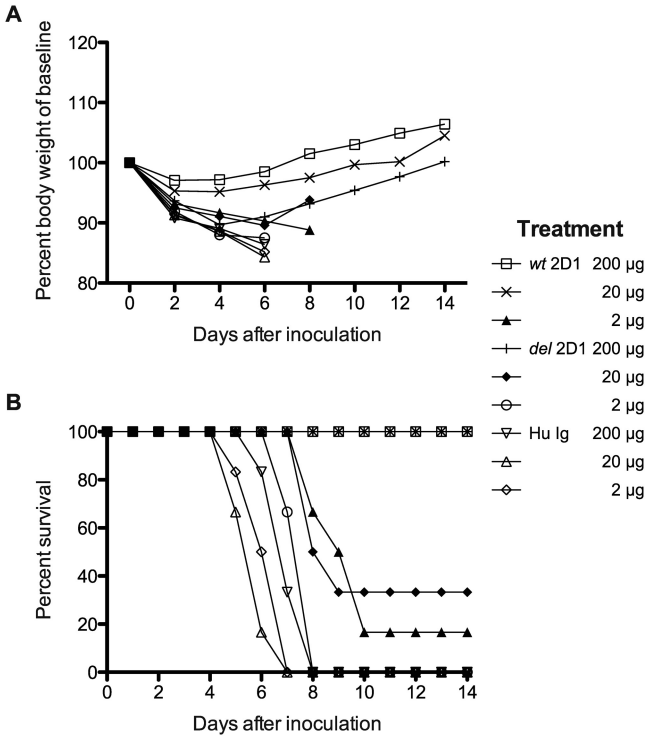

FIG 3 Therapeutic efficacy of 1918 HA-specific MAbs against disease caused by the 1918 A(H1N1) virus in mice. Mice were inoculated on day 0 and treated on day 1 with the indicated antibody and dose. In each group, six mice were monitored every other day for weight (A) and survival (B).

Interestingly, the three-amino-acid insertion in *wt* 2D1 lies in the middle of the β-strand immediately following CDR H2, which is part of the core of the immunoglobulin fold. Unlike insertions in the turns, which can easily be accommodated by extending loop length, insertion in the middle of a strand is more drastic, requiring either a bulge outward from the face of the β-sheet or a shift in the register of the strand that displaces the inserted residues toward the loop at either end. In *wt* 2D1, the insertion at the CDR H2-FR3 junction triggers a shift in the register of the strand in both directions from the point of insertion, with one amino acid shifted N terminally, toward the tip of CDR H2, while the other two inserted residues displace the rest of the strand C terminally toward the turn at the opposite end, adjacent to the Fab constant domains. The introduction of a single amino acid bulge in the tip of CDR H2 results in a clash between CDRs H1 and H2, leading to a distortion of H1 and a modular shift of the loop away from interaction with the HA surface. Thus, removal of the insertion would be expected to restore the proper register of the β-strand and relieve the bulge from the tip of CDR H2, thereby allowing CDR H1 to relax back into the more compact conformation observed in other Fab structures. This hypothesis is confirmed by the structure of *del* 2D1 Fab, which lacks the three-amino-acid insertion. As expected, the canonical configurations of CDRs H1 and

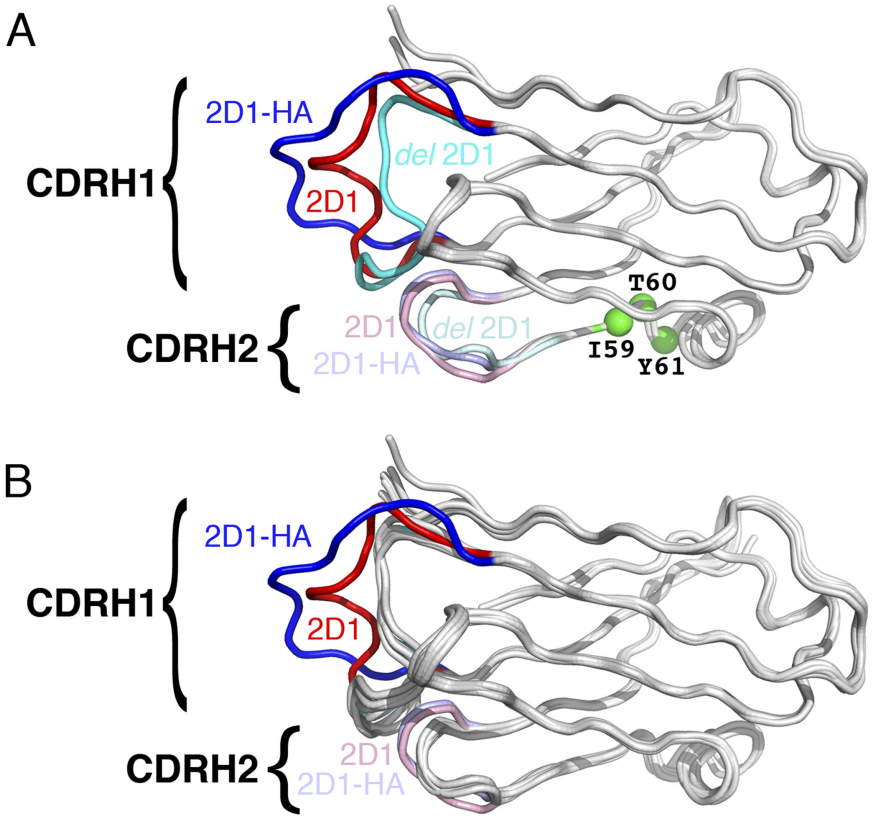

FIG 4 Insertion in 2D1 remodels the combining site loop architecture. (A) Superposition of V_H gene-derived regions from HA-bound *wt* 2D1 (PDB code 3LZF), free *wt* 2D1 Fab (PDB code 3QHZ), and free *del* 2D1 (PDB code 3QHF). CDR H1 is highlighted in blue (2D1-HA complex), red (unbound *wt* 2D1 Fab), and cyan (unbound *del* 2D1 Fab), with H2 in lighter shades. The ITY insertion (green spheres in the *wt* 2D1 structures) triggers a register shift in the strand and an extension of CDR H2. This extended loop impinges upon CDR H1, forcing it out of its usual position into the more open, extended conformations observed in *wt* 2D1. (B) Same depiction as in panel A but also showing the superposition of the five most closely related Fab structures from the PDB (on the basis of V_H sequence similarity [PDB codes 2HWZ, 2AGJ, 3IFL, 1U92, and 2ROZ]). *del* 2D1 lies near the center of the cluster of related structures and is not easily visible. Thus, simply reverting the ITY insertion to the germ line sequence is sufficient to restore the expected CDR H1 and H2 conformations.

H2 are restored and the structure of *del* 2D1 closely resembles that of sequence-related Fabs (Fig. 4B).

Comparison of the structure of *del* 2D1 with that of the *wt* 2D1/1918 HA complex explains how the three-amino-acid insertion in *wt* 2D1 at the junction of CDR H2 and FR3 caused enhancement of antibody binding and function. Without the insertion, interaction of *del* 2D1 Fab with the HA protein is compromised by a steric clash between the common, compact configuration of CDR H1 and the target epitope on the HA antigen (Fig. 5). The insertion in *wt* 2D1 mediates a bulge in the CDR H2 loop that, in turn, impinges upon the base of CDR H1, resulting in the displacement of CDR H1 away from the HA surface, thus resolving steric clashes with the HA.

DISCUSSION

We show here that a novel insertion coupled with somatic point mutations in a human antibody framework region mediated a major enhancement of binding and antiviral activity by second-shell effects modulating the conformation and spatial disposition of the heavy-chain CDR loops. The case of MAb 2D1 highlights several interesting principles that may be important in antibody affinity maturation and the generation of neutralizing antibodies. First, the effect of the insertion was indirect. Rather than altering CDR H1 directly to relieve a steric clash, an insertion near the CDR H2 loop was selected that affected binding principally by altering the orientation and relative disposition of the adjacent CDR H1 loop. Second, the effect of the insertion was surprising in that the mechanism was subtractive. The CDR H1 displacement resolved a steric conflict in the parental antibody-antigen interaction by moving a CDR away from the region of interaction, rather than mediating a new interaction in the antibody-antigen interface. While perhaps underappreciated, removing conflicting and unfavorable interactions may be nearly as important during affinity maturation as adding favorable ones.

Insertions and deletions in antibody gene sequences have been noted previously in reports on a subset of sequences in antibody genes from memory B cells in lymphoid tissues, such as lymph node, spleen, or synovial tissue (1–3, 5). The percentage of memory cells with gene sequences containing insertions or deletions was low (1.3 to 6.5% in previous reports [1, 3, 5, 20]), although the true frequency is not well defined because of the small numbers of cells that have been tested to date. These novel alterations appear to result from DNA duplication events following DNA strand breaks during the somatic hypermutation process. Many of the insertions noted previously occurred at mutational hot spots for error-prone DNA polymerases. Previous reports have established that insertions and deletions contribute to the genetic diversity of the antibody repertoire at the DNA level, but it is less clear if such alterations mediate structural or functional changes that enhance binding to the corresponding epitope. The data in this paper show that complex structural rearrangements mediated by an insertion/deletion event can markedly enhance the binding and function of a human antibody against a major human pathogen.

Somatic hypermutation requires both hot spot-directed and randomly directed processes (21). Somatic mutation hot spots correspond to the error spectrum of DNA polymerase η (14). The motif D**G**YW (D = A/G/T), its reverse complement WRCH (14, 15, 20), and the WA motif (14) are predictors of high mutability in immunoglobulin hypermutation. The insertion that is observed in *wt* 2D1 appears to be a result of a point mutation at a conventional WA motif, followed by an insertion that occurred at the site of the motif WRCH that was introduced by the prior point mutation. The activation-induced (cytidine) deaminase (AID) enzyme is important for both class switch recombination and somatic

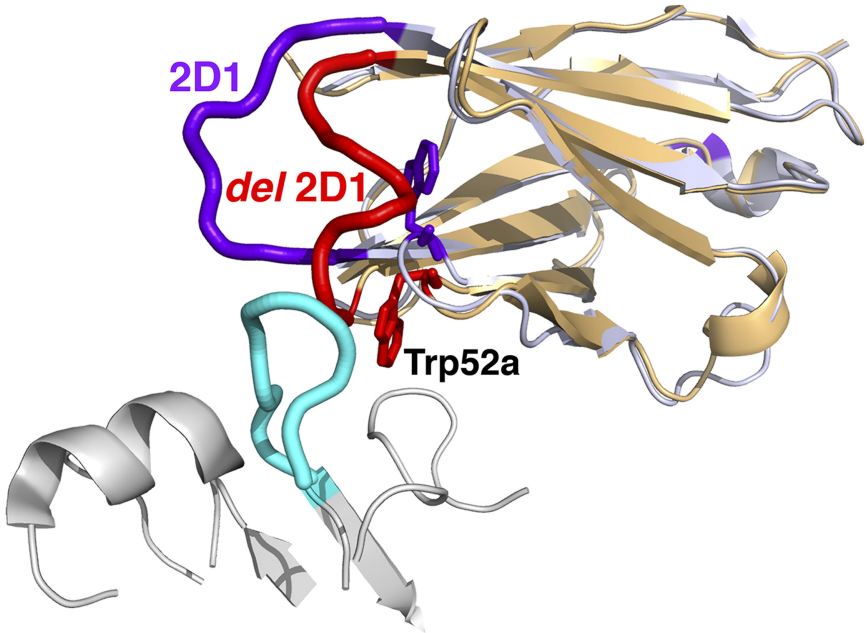

FIG 5 Combining site reconfiguration due to ITY insertion relieves potential steric clashes between the epitope on HA (bottom left in grey and cyan) and antibody CDRs (top right). Superposition of *del* 2D1 Fab onto the *wt* 2D1-HA complex structure, with Fabs oriented approximately as in Fig. 4. In the germ line configuration, the base of CDR H1 and the Trp52a side chain from CDR H2 would be in conflict with an HA epitope loop. The ITY insertion and extended CDR H2 in *wt* 2D1 push Trp52a up and away from the epitope, simultaneously displacing CDR H1 from its usual position, allowing *wt* 2D1 to recognize HA in a manner that is otherwise unfavorable for the germ line Fab.

hypermutation (29, 30), catalyzing dC → dU deamination most avidly on double-stranded DNA substrates containing a small "transcription-like" single-stranded DNA bubble (31). The resultant mismatch can lead to widespread DNA double-strand breaks during times of high levels of transcription of antibody genes (32) which can be repaired by nonhomologous end joining (33), which would be an alternate explanation for the ins/del events described here.

We showed previously that MAb 2D1 binds to and neutralizes the 1918 and 2009 pandemic H1N1 viruses (13). Here, we also show that MAb 2D1 did not show HAI activity against recent seasonal H1N1 viruses, as would be expected based on the presence of glycosylation sites within the Sa site of such viruses (12). *del* 2D1 bound 1918 HA about 35-fold less well than *wt* 2D1. Likewise, the HAI activity of *del* 2D1 against the 1918 or 2009 pandemic virus was reduced 4-fold compared to that of *wt* 2D1. *del* 2D1 also was less active in an *in vivo* model of therapeutic efficacy. These findings suggested that the insertion within *wt* 2D1 was critical for the acquisition of high potency of the antibody.

Interestingly, the insertion in *wt* 2D1 is within a β-sheet. This is surprising, as random insertions or deletions in β-sheets often would result in the disruption of this secondary structure and perhaps destabilize the protein or interfere with folding. Here, a three-amino-acid insertion was accommodated by a register shift in the β-sheet and by a change in the conformation of the adjacent loop. The crystal structures presented here suggest that this insertion in *wt* 2D1 does not, in fact, lead to a "bulge" in the buried β-sheet at the site of insertion but results in the displacement of three residues encoded in the germ line sequence to cause a bulge in the external loop of CDR H2. Subsequently, this alteration resulted in the displacement of heavy-chain CDR H1 in the *wt* structure, a feature not present in *del* 2D1. Heavy-chain CDR H1 of *wt* 2D1 does not participate in the interaction with the HA antigen (12). However, heavy-chain CDR H2 is located directly at the interface, and it seems that the insertion near CDR H2 improves the interaction, mainly by removing CDR H1 from the interacting region.

In conclusion, these studies show that a somatic insertion/deletion can dramatically impact both the structure and the function of the resulting antibody. This molecular mechanism may constitute a major component of the diversification and enhancement of high-potency antibodies in the human antibody repertoire.

MATERIALS AND METHODS

Expression and purification of *wt* 2D1 and *del* 2D1. To prepare *del* 2D1 Fab or IgG1, we used recombinant expression in mammalian cells as previously described (12). Briefly, the MAb 2D1 heavy- and light-chain genes were cloned into the pEE6.4 and pEE12.4 vectors, respectively (Lonza). For production of Fabs, a stop codon was introduced into the heavy-chain gene immediately after the codon for the cysteine of the hinge disulfide. The QuikChange Primer design tool (Agilent) was used to design site-directed mutagenesis primers (Invitrogen) to create a cDNA encoding *del* 2D1 using the QuikChange II XL kit. The plasmid bearing the *del* 2D1 heavy-chain gene was transformed into XL10-gold cells for EndoFree Plasmid Maxi DNA preparation (Qiagen) after sequence verification (Vanderbilt DNA Sequencing Facility). A plasmid encoding the *wt* 2D1 light chain was used for both MAbs. Heavy- and light-chain DNAs were cotransfected transiently into HEK 293 F cells (Invitrogen) using PolyFect reagent (Qiagen), and the cells were incubated in humidified air with CO_2 in shaker flasks. The supernatant was harvested, purified, and concentrated as previously described (12).

Biosensor studies. The binding affinity of recombinant *wt* 2D1 and *del* 2D1 Fabs for recombinant, trimerized, His-tagged HA protein containing the sequence from the influenza virus A/South Carolina/1/1918 strain was measured using anti-Penta-HIS tips on the Octet QK platform (FortéBio, Menlo Park, CA). Soluble HA protein was expressed and purified as previously described (13).

HAI assays. HAI tests using full-length recombinant purified MAbs were performed according to standard protocols (22). Briefly, serial dilutions of purified MAbs in phosphate-buffered saline (PBS) were prepared from an initial concentration of 5 μg/ml. Sera were initially diluted 1:10 in receptor-destroying enzyme from *Vibrio cholerae* (Denka Seiken). Serial dilutions of mouse positive-control sera or human MAbs were preincubated with four HA units of virus per well. Turkey red blood cells (RBCs) were added to a final concentration of 0.5%, and the plate was incubated at room temperature for 30 to 60 min. Serum titers were expressed as the reciprocal of the highest dilution of serum inhibiting the agglutination of 0.5% of the RBCs at 4 HA units of virus. Normal mouse serum gave a value of less than 10. The specific HAI activity of a MAb was calculated as the lowest concentration of the MAb that displayed HAI activity.

Animal studies. Female 8-week-old BALB/c mice were inoculated intranasally with 1,000 50% mouse infectious doses in a 50-μl volume of the virulent reconstituted 1918 virus as previously described (6). At 24 h after inoculation, mice were each administered 200, 20, or 2 μg (approximately

10, 1, or 0.1 mg/kg) of *del* 2D1 or *wt* 2D1 MAb or an equal volume of human IgG (Sigma) by the intraperitoneal route in groups of 10 mice. Mice were observed for weight loss every other day for 14 days. Subsets of four animals treated with MAbs were euthanized on day 3 after infection, and whole lungs were homogenized in 1 ml of sterile PBS. Virus titers in lung tissue homogenates were determined by plaque titration in MDCK cell monolayer cultures. The limit of virus detection was $10^{0.95}$. Statistical analyses were performed with R (the R Project for Statistical Computing). Survival distributions between antibody-treated groups were compared using the nonparametric log-rank test. The Wilcoxon signed-rank test was used to compare virus titers, which cannot be assumed to be normally distributed.

Crystallization and structure determination of *wt* 2D1 and *del* 2D1. *wt* 2D1 Fab was generated by proteolysis of intact IgG with endoproteinase Lys-C. Recombinant *del* 2D1 Fab was expressed as described above, with a stop codon in the heavy-chain constant domain after the cysteine codon in the hinge disulfide region. Fab proteins were purified by affinity chromatography using CaptureSelect lambda resin (BAC B.V.). The eluted material was buffer transferred to 50 mM sodium acetate buffer, pH 5.0, and subjected to cation-exchange chromatography using a MonoS resin (GE Healthcare). After a final gel filtration step to remove any aggregates, the Fabs were concentrated to approximately 15 mg/ml and screened for crystallization conditions using the robotic Crystalmation platform at the Joint Center for Structural Genomics (JCSG). Crystals for each Fab were obtained under several conditions. Crystals for diffraction data collection were grown at 20°C in sitting drops by vapor diffusion with a reservoir containing 22% PEG 4000 and 150 mM calcium acetate (*wt* 2D1) or 20% PEG 4000, 100 mM sodium acetate, and 200 mM magnesium acetate (*del* 2D1). Crystals were cryoprotected by the addition of 20% glycerol to the mother liquor and flash cooled by plunging into liquid nitrogen.

Diffraction data were collected at the Stanford Synchrotron Radiation Lightsource (SSRL) beam line 9-2 (*wt* 2D1) and the Advanced Photon Source (APS) NIH Medicine and Cancer Institutes Collaborative Access Team (GM/CA-CAT) beam line 23ID-D (*del* 2D1) at the Argonne National Laboratory. Diffraction data were integrated, scaled, and merged in HKL2000 (HKL Research). The structures were solved by molecular replacement using Phaser (23). The 1918 virus-bound 2D1 coordinates (PDB code 3LZF) were used as a search model for *wt* 2D1 Fab, which was in turn used to phase the *del* 2D1 data set. In each case, CDRs H1 and H3 were pruned before molecular replacement to minimize model bias. The *wt* 2D1 and *del* 2D1 structures contain two copies and one copy of the Fab in the asymmetric unit, respectively. The *wt* 2D1 and *del* 2D1 coordinates were refined in Phenix (24), including simulated annealing and translation-libration-screw (TLS) with one group for each Ig domain. The models were adjusted, the CDRs were rebuilt, and waters were added in the late stages of refinement using Coot (25). The models were validated using the JCSG Quality Control Server (version 2.7, publicly available at http://smb.slac.stanford.edu/jcsg/QC/), which includes Molprobity (26). Kabat numbering of the Fabs was assigned by the AbNum web server (http://www.bioinf.org.uk/abs/abnum) (27), with modification for 2D1 to accommodate the insertion, as discussed by Xu et al. (12). Final data collection and refinement statistics can be found in Table S1 in the supplemental material.

Sequence accession numbers. Coordinates and structure factors for *wt* 2D1 and *del* 2D1 have been deposited in the Protein Data Bank (PDB codes 3QHZ and 3QHF, respectively).

ACKNOWLEDGMENTS

This work was supported by NIH grant P01 AI058113, Department of Defense grant HDTRA1-08-10-BRCWMD-BAA, and the Skaggs Institute for Chemical Biology. J.C.K. was supported by a Pediatric Infectious Diseases Society fellowship award. J.E.C. is a Burroughs Wellcome Fund clinical scientist in translational research. D.C.E. acknowledges predoctoral support from the Achievement Rewards for College Scientists Foundation and the NIH Molecular Evolution Training Program (GM080209).

Portions of this research were also carried out at the Stanford Synchrotron Radiation Laboratory, a national user facility operated by Stanford University on behalf of the U.S. Department of Energy, Office of Basic Energy Sciences. The SSRL Structural Molecular Biology Program is supported by the Department of Energy, Office of Biological and Environmental Research, and by the National Institutes of Health, National Center for Research Resources, Biomedical Technology Program, and the National Institute of General Medical Sciences. GM/CA-CAT has been funded in whole or in part with federal funds from the National Cancer Institute (Y1-CO-1020) and the National Institute of General Medical Sciences (Y1-GM-1104). Use of the Advanced Photon Source was supported by the U.S. Department of Energy, Basic Energy Sciences, Office of Science, under contract DE-AC02-06CH11357.

We thank Kimberly Crimin for help with the statistical analysis, Chelsey J. Huffman and Frances House (Vanderbilt University) for excellent technical support, Henry Tien and David Marciano for assistance with robotic crystallization experiments at the JCSG, Nagarajan Venugopalan and the staff of the APS GM/CA-CAT 23ID-D for beam line support, and Robyn Stanfield, Xiaoping Dai, and Marc-André Elsliger for assistance with data collection and refinement and helpful discussions.

The findings and conclusions in this report are ours and do not necessarily reflect the views of the funding agency.

SUPPLEMENTAL MATERIAL

Supplemental material for this article may be found at http://mbio.asm.org/lookup/suppl/doi:10.1128/mBio.00345-10/-/DCSupplemental.

Table S1, DOC file, 0.051 MB.

REFERENCES

1. **de Wildt, R. M., W. J. van Venrooij, G. Winter, R. M. Hoet, and I. M. Tomlinson.** 1999. Somatic insertions and deletions shape the human antibody repertoire. J. Mol. Biol. **294**:701–710.
2. **Miura, Y., C. C. Chu, D. M. Dines, S. E. Asnis, R. A. Furie, and N. Chiorazzi.** 2003. Diversification of the Ig variable region gene repertoire of synovial B lymphocytes by nucleotide insertion and deletion. Mol. Med. **9**:166–174.
3. **Wilson, P. C., O. de Bouteiller, Y. J. Liu, K. Potter, J. Banchereau, J. D. Capra, and V. Pascual.** 1998. Somatic hypermutation introduces insertions and deletions into immunoglobulin V genes. J. Exp. Med. **187**:59–70.
4. **Jacobs, H., Y. Fukita, G. T. van der Horst, J. de Boer, G. Weeda, J. Essers, N. de Wind, B. P. Engelward, L. Samson, S. Verbeek, J. M. de Murcia, G. de Murcia, H. te Riele, and K. Rajewsky.** 1998. Hypermutation of immunoglobulin genes in memory B cells of DNA repair-deficient mice. J. Exp. Med. **187**:1735–1743.
5. **Goossens, T., U. Klein, and R. Kuppers.** 1998. Frequent occurrence of deletions and duplications during somatic hypermutation: implications for oncogene translocations and heavy chain disease. Proc. Natl. Acad. Sci. U. S. A. **95**:2463–2468.
6. **Yu, X., T. Tsibane, P. A. McGraw, F. S. House, C. J. Keefer, M. D. Hicar, T. M. Tumpey, C. Pappas, L. A. Perrone, O. Martinez, J. Stevens, I. A. Wilson, P. V. Aguilar, E. L. Altschuler, C. F. Basler, and J. E. Crowe, Jr.** 2008. Neutralizing antibodies derived from the B cells of 1918 influenza pandemic survivors. Nature **455**:532–536.
7. **Tumpey, T. M., C. F. Basler, P. V. Aguilar, H. Zeng, A. Solorzano, D. E. Swayne, N. J. Cox, J. M. Katz, J. K. Taubenberger, P. Palese, and A. Garcia-Sastre.** 2005. Characterization of the reconstructed 1918 Spanish influenza pandemic virus. Science **310**:77–80.
8. **Fraser, C., C. A. Donnelly, S. Cauchemez, W. P. Hanage, M. D. Van Kerkhove, T. D. Hollingsworth, J. Griffin, R. F. Baggaley, H. E. Jenkins, E. J. Lyons, T. Jombart, W. R. Hinsley, N. C. Grassly, F. Balloux, A. C. Ghani, N. M. Ferguson, A. Rambaut, O. G. Pybus, H. Lopez-Gatell, C. M. Alpuche-Aranda, I. B. Chapela, E. P. Zavala, D. M. Guevara, F. Checchi, E. Garcia, S. Hugonnet, and C. Roth.** 2009. Pandemic potential of a strain of influenza A (H1N1): early findings. Science **324**:1557–1561.
9. **Brownlee, G. G., and E. Fodor.** 2001. The predicted antigenicity of the haemagglutinin of the 1918 Spanish influenza pandemic suggests an avian origin. Philos. Trans. R. Soc. Lond. B Biol. Sci. **356**:1871–1876.
10. **Caton, A. J., G. G. Brownlee, J. W. Yewdell, and W. Gerhard.** 1982. The antigenic structure of the influenza virus A/PR/8/34 hemagglutinin (H1 subtype). Cell **31**:417–427.

11. **Wilson, I. A., J. J. Skehel, and D. C. Wiley.** 1981. Structure of the haemagglutinin membrane glycoprotein of influenza virus at 3 Ä resolution. Nature **289**:366–373.
12. **Xu, R., D. C. Ekiert, J. C. Krause, R. Hai, J. E. Crowe, Jr., and I. A. Wilson.** 2010. Structural basis of preexisting immunity to the 2009 H1N1 pandemic influenza virus. Science **328**:357–360.
13. **Krause, J. C., T. M. Tumpey, C. J. Huffman, P. A. McGraw, M. B. Pearce, T. Tsibane, R. Hai, C. F. Basler, and J. E. Crowe, Jr.** 2010. Naturally occurring human monoclonal antibodies neutralize both 1918 and 2009 pandemic influenza A (H1N1) viruses. J. Virol. **84**:3127–3130.
14. **Rogozin, I. B., Y. I. Pavlov, K. Bebenek, T. Matsuda, and T. A. Kunkel.** 2001. Somatic mutation hotspots correlate with DNA polymerase eta error spectrum. Nat. Immunol. **2**:530–536.
15. **Rogozin, I. B., and M. Diaz.** 2004. Cutting edge: DGYW/WRCH is a better predictor of mutability at G:C bases in Ig hypermutation than the widely accepted RGYW/WRCY motif and probably reflects a two-step activation-induced cytidine deaminase-triggered process. J. Immunol. **172**:3382–3384.
16. **Garten, R. J., C. T. Davis, C. A. Russell, B. Shu, S. Lindstrom, A. Balish, W. M. Sessions, X. Xu, E. Skepner, V. Deyde, M. Okomo-Adhiambo, L. Gubareva, J. Barnes, C. B. Smith, S. L. Emery, M. J. Hillman, P. Rivailler, J. Smagala, M. de Graaf, D. F. Burke, R. A. Fouchier, C. Pappas, C. M. Alpuche-Aranda, H. Lopez-Gatell, H. Olivera, I. Lopez, C. A. Myers, D. Faix, P. J. Blair, C. Yu, K. M. Keene, P. D. Dotson, Jr., D. Boxrud, A. R. Sambol, S. H. Abid, K. St. George, T. Bannerman, A. L. Moore, D. J. Stringer, P. Blevins, G. J. Demmler-Harrison, M. Ginsberg, P. Kriner, S. Waterman, S. Smole, H. F. Guevara, E. A. Belongia, P. A. Clark, S. T. Beatrice, R. Donis, J. Katz, L. Finelli, C. B. Bridges, M. Shaw, D. B. Jernigan, T. M. Uyeki, D. J. Smith, A. I. Klimov, and N. J. Cox.** 2009. Antigenic and genetic characteristics of swine-origin 2009 A(H1N1) influenza viruses circulating in humans. Science **325**:197–201.
17. **Maines, T. R., A. Jayaraman, J. A. Belser, D. A. Wadford, C. Pappas, H. Zeng, K. M. Gustin, M. B. Pearce, K. Viswanathan, Z. H. Shriver, R. Raman, N. J. Cox, R. Sasisekharan, J. M. Katz, and T. M. Tumpey.** 2009. Transmission and pathogenesis of swine-origin 2009 A(H1N1) influenza viruses in ferrets and mice. Science **325**:484–487.
18. **Munster, V. J., E. de Wit, J. M. van den Brand, S. Herfst, E. J. Schrauwen, T. M. Bestebroer, D. van de Vijver, C. A. Boucher, M. Koopmans, G. F. Rimmelzwaan, T. Kuiken, A. D. Osterhaus, and R. A. Fouchier.** 2009. Pathogenesis and transmission of swine-origin 2009 A(H1N1) influenza virus in ferrets. Science **325**:481–483.
19. **Belser, J. A., D. A. Wadford, C. Pappas, K. M. Gustin, T. R. Maines, M. B. Pearce, H. Zeng, D. E. Swayne, M. Pantin-Jackwood, J. M. Katz, and T. M. Tumpey.** 2010. Pathogenesis of pandemic influenza A (H1N1) and triple-reassortant swine influenza A (H1) viruses in mice. J. Virol. **84**:4194–4203.
20. **Dorner, T., S. J. Foster, N. L. Farner, and P. E. Lipsky.** 1998. Somatic hypermutation of human immunoglobulin heavy chain genes: targeting of RGYW motifs on both DNA strands. Eur. J. Immunol. **28**:3384–3396.
21. **Weitkamp, J. H., N. L. Kallewaard, A. L. Bowen, B. J. Lafleur, H. B. Greenberg, and J. E. Crowe, Jr.** 2005. VH1-46 is the dominant immunoglobulin heavy chain gene segment in rotavirus-specific memory B cells expressing the intestinal homing receptor alpha4beta7. J. Immunol. **174**:3454–3460.
22. **Kendal, A. P., J. J. Skehel, and M. S. Pereira.** 1982. Concepts and procedures for laboratory-based influenza surveillance. Publication no. B17–35. Centers for Disease Control, Atlanta, GA.
23. **McCoy, A. J., R. W. Grosse-Kunstleve, L. C. Storoni, and R. J. Read.** 2005. Likelihood-enhanced fast translation functions. Acta Crystallogr. D Biol. Crystallogr. **61**:458–464.
24. **Adams, P. D., R. W. Grosse-Kunstleve, L. W. Hung, T. R. Ioerger, A. J. McCoy, N. W. Moriarty, R. J. Read, J. C. Sacchettini, N. K. Sauter, and T. C. Terwilliger.** 2002. PHENIX: building new software for automated crystallographic structure determination. Acta Crystallogr. D Biol. Crystallogr. **58**:1948–1954.
25. **Emsley, P., B. Lohkamp, W. G. Scott, and K. Cowtan.** 2010. Features and development of Coot. Acta Crystallogr. D Biol. Crystallogr. **66**:486–501.
26. **Davis, I. W., A. Leaver-Fay, V. B. Chen, J. N. Block, G. J. Kapral, X. Wang, L. W. Murray, W. B. Arendall III, J. Snoeyink, J. S. Richardson, and D. C. Richardson.** 2007. MolProbity: all-atom contacts and structure validation for proteins and nucleic acids. Nucleic Acids Res. **35**:W375–W383.
27. **Abhinandan, K. R., and A. C. Martin.** 2008. Analysis and improvements to Kabat and structurally correct numbering of antibody variable domains. Mol. Immunol. **45**:3832–3839.
28. **Ruiz, M., and M. P. Lefranc.** 2002. IMGT gene identification and Colliers de Perles of human immunoglobulins with known 3D structures. Immunogenetics **53**:857–883.
29. **Muramatsu, M., K. Kinoshita, S. Fagarasan, S. Yamada, Y. Shinkai, and T. Honjo.** 2000. Class switch recombination and hypermutation require activation-induced cytidine deaminase (AID), a potential RNA editing enzyme. Cell **102**:553–563.
30. **Revy, P., T. Muto, Y. Levy, F. Geissmann, A. Plebani, O. Sanal, N. Catalan, M. Forveille, R. Dufourcq-Labelouse, A. Gennery, I. Tezcan, F. Ersoy, H. Kayserili, A. G. Ugazio, N. Brousse, M. Muramatsu, L. D. Notarangelo, K. Kinoshita, T. Honjo, A. Fischer, and A. Durandy.** 2000. Activation-induced cytidine deaminase (AID) deficiency causes the autosomal recessive form of the Hyper-IgM syndrome (HIGM2). Cell **102**:565–575.
31. **Bransteitter, R., P. Pham, M. D. Scharff, and M. F. Goodman.** 2003. Activation-induced cytidine deaminase deaminates deoxycytidine on single-stranded DNA but requires the action of RNase. Proc. Natl. Acad. Sci. USA **100**:4102–4107.
32. **Hasham, M. G., N. M. Donghia, E. Coffey, J. Maynard, K. J. Snow, J. Ames, R. Y. Wilpan, Y. He, B. L. King, and K. D. Mills.** 2010. Widespread genomic breaks generated by activation-induced cytidine deaminase are prevented by homologous recombination. Nat. Immunol. **11**:820–826.
33. **Difilippantonio, S., E. Gapud, N. Wong, C. Y. Huang, G. Mahowald, H. T. Chen, M. J. Kruhlak, E. Callen, F. Livak, M. C. Nussenzweig, B. P. Sleckman, and A. Nussenzweig.** 2008. 53BP1 facilitates long-range DNA end-joining during V(D)J recombination. Nature **456**:529–533.